JVST A
Journal of Vacuum Science & Technology A

Germanium dioxide: A new rutile substrate for epitaxial film growth

Cite as: J. Vac. Sci. Technol. A **40**, 050401 (2022); https://doi.org/10.1116/6.0002011
Submitted: 08 June 2022 • Accepted: 26 July 2022 • Published Online: 31 August 2022

Sieun Chae, Lucas A. Pressley, Hanjong Paik, et al.

JVST A
Journal of Vacuum Science & Technology A

ARTICLE

avs.scitation.org/journal/jva

Germanium dioxide: A new rutile substrate for epitaxial film growth

Cite as: J. Vac. Sci. Technol. A **40**, 050401 (2022); doi: 10.1116/6.0002011
Submitted: 8 June 2022 · Accepted: 26 July 2022 ·
Published Online: 31 August 2022

Sieun Chae,[1] Lucas A. Pressley,[2,3] Hanjong Paik,[4] Jiseok Gim,[1] Don Werder,[4] Berit H. Goodge,[5] Lena F. Kourkoutis,[5,6] Robert Hovden,[1] Tyrel M. McQueen,[2,3,7] Emmanouil Kioupakis,[1] and John T. Heron[1,a)]

AFFILIATIONS

[1]Department of Materials Science and Engineering, University of Michigan, Ann Arbor, Michigan 48109
[2]Department of Chemistry, The Johns Hopkins University, Baltimore, Maryland 21218
[3]The William H. Miller III Department of Physics and Astronomy, Institute for Quantum Matter, The Johns Hopkins University, Baltimore, Maryland 21218
[4]Platform for the Accelerated Realization, Analysis, and Discovery of Interface Materials (PARADIM), Cornell University, Ithaca, New York 14853
[5]School of Applied and Engineering Physics, Cornell University, Ithaca, New York 14853
[6]Kavli Institute at Cornell for Nanoscale Science, Cornell University, Ithaca, New York 14853
[7]Department of Materials Science and Engineering, The Johns Hopkins University, Baltimore, Maryland 21218

Note: This paper is a part of the Special Topic Collection on Thin Film Deposition for Materials Discovery.
[a)]**Author to whom correspondence should be addressed:** jtheron@umich.edu

ABSTRACT

Rutile compounds have exotic functional properties that can be applied for various electronic applications; however, the limited availability of epitaxial substrates has restricted the study of rutile thin films to a limited range of lattice parameters. Here, rutile GeO_2 is demonstrated as a new rutile substrate with lattice parameters of $a = 4.398$ Å and $c = 2.863$ Å. Rutile GeO_2 single crystals up to 4 mm in size are grown by the flux method. X-ray diffraction reveals high crystallinity with a rocking curve having a full width half-maximum of 0.0572°. After mechanical polishing, a surface roughness of less than 0.1 nm was obtained, and reflection high-energy electron diffraction shows a crystalline surface. Finally, epitaxial growth of (110)-oriented TiO_2 thin films on GeO_2 substrates was demonstrated using molecular beam epitaxy. Templated by rutile GeO_2 substrates, our findings open the possibility of stabilizing new rutile thin films and strain states for the tuning of physical properties.

I. INTRODUCTION

Rutile (space group $P4_2/mnm$) is a tetragonal crystal structure of MX_2 (X = O, F) stoichiometry in which cations are octahedrally coordinated with an edge-sharing octahedron network along the c axis. Rutile-type ionic compounds are characterized by a closely packed lattice, high crystal symmetry, and anisotropic material properties perpendicular and parallel to the c direction. The rutile structure accommodates a wide range of cations and has shown exotic functional properties. For example, VO_2 and NbO_2 are metallic in the rutile structure but exhibit a metal-to-insulator transition driven by their inherent structural instability which is harnessed in phase-transition field-effect transistors.[1,2] Rutile TiO_2 and SnO_2 are technically important wide-bandgap semiconductors widely applied in photocatalysts, photovoltaic devices, and gas-sensors.[3–5] RuO_2 and IrO_2 are major oxygen evolution electrocatalysts and their applications range from catalysts to supercapacitors and battery anodes.[6,7] The properties of these films (critical temperature, resistance, photon energy, catalytic activity, etc.) are strain tunable, which allows for tunability in the epitaxial thin films for a target property.[8–12]

Although epitaxial thin film growth of rutile crystals has been demonstrated on numerous substrates, TiO_2 and MgF_2 are among

the few commercial substrates having a rutile crystal structure. Though rutile compounds exist in a wide range of lattice parameters (Fig. 1), the limited availability of isostructural substrates suitable for epitaxial deposition has limited the synthesis of rutile compounds with high crystallinity or optimal strain tuning of properties. For instance, due to the presence of multiple oxidation states and polytypes, compounds such as MnO_2 or CrO_2 require suitable templating substrates to stabilize the metastable rutile phase. Nevertheless, owing to the relatively large lattice misfit with TiO_2 (the *a* lattice mismatch of 4.3%), rutile MnO_2 has only been stabilized up to 20 nm thickness on a rutile TiO_2 substrate with an interfacial Ti diffusion self-adapting layer.[13,14] Similarly, the deposition of CrO_2 on TiO_2 (the *a* lattice mismatch of 3.8%) is accompanied by the incorporation of Cr_2O_3 phases.[15] On the other hand, an MgF_2 substrate complicates the growth of oxide thin films as the surface termination of fluorine often challenges the interfacial bonding of oxides. Sapphire also templates epitaxial rutile films due to the coincidence of the atomic configuration in certain planes. The reported orientational relationships between the rutile films and sapphire substrates are (101)//(1$\bar{1}$02), (001)//(10$\bar{1}$0), (100)//(0001), and ($\bar{1}$01)//(11$\bar{2}$0).[16,17] Nevertheless, rutile and sapphire have different crystal structures (tetragonal and hexagonal, respectively) and the axial ratio (*c*/*a*) of the sapphire deviates from the general trend of the rutile compounds necessitating lattice misfit strains (Fig. 1), which reduces the film crystallinity compared to films grown on isostructural substrates.[18] Therefore, a new rutile substrate with distinct lattice constants can open new possibilities for films and strain states.

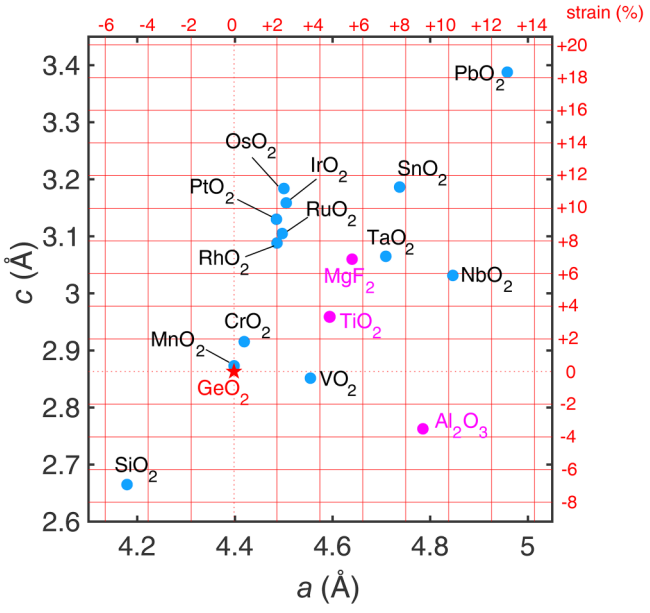

FIG. 1. *a* and *c* lattice parameters of rutile compounds. The grid line indicates misfit strain with respect to GeO_2 substrates. TiO_2, MgF_2, and Al_2O_3 are commercially available rutile substrates. A GeO_2 substrate provides a low lattice mismatch to MnO_2, CrO_2, and VO_2 (along the *c* direction) and allows compressive strain states for RuO_2, IrO_2, and VO_2. The lattice parameters of Al_2O_3 are chosen to meet the epitaxial relation with the rutile structure (the *a* lattice parameter is the *a* lattice parameter in the hexagonal conventional cell of Al_2O_3 and the *c* lattice parameter is $a/\sqrt{3}$). Data were taken from Ref. 1.

Rutile GeO_2 (r-GeO_2) is water-insoluble and thermodynamically the most stable phase of GeO_2 with the *a* and *c* lattice parameters of 4.398 and 2.863 Å, respectively.[19] r-GeO_2 single-crystal substrates have potential advantages as follows. First, the large lattice constant difference of GeO_2 with TiO_2 and MgF_2 (4.3% and 5.2%, respectively, along the *a* axis) can potentially allow the epitaxial stabilization of new films that are otherwise challenging to grow on a TiO_2 substrate. It can also enable the exploration of novel functional properties of known compounds by opening new regions of strain space. For example, it has been discovered that epitaxial strain is a promising strategy to create superconductivity of rutile RuO_2 as the (110) in-plane strain enhances the density of states near the Fermi level.[10] r-GeO_2 has an ultrawide bandgap of 4.68 eV and is electrically insulating in the absence of intentional dopants,[20] which allows electrical and optical characterization of narrower-gap thin films unaffected by substrate properties. While TiO_2 substrates can lose oxygen during deposition which commonly leads to high electrical conductivity,[21,22] r-GeO_2 does not suffer from conductivity change during deposition as oxygen vacancy energy level lies deep in the bandgap and r-GeO_2 does not favor the formation of oxygen-deficient phases.[20,23] Various bulk synthesis techniques, such as Czochralski and vapor transport, have been attempted to realize r-GeO_2 single crystals; however, the crystal size ranges from 0.5 to 2 mm which limits their application as epitaxial film growth substrates.[24,25]

Here, we showcase $4 \times 2\ mm^2$ rutile GeO_2 single-crystal substrates with highly crystalline surfaces that can be used for epitaxial film growth. Millimeter-size r-GeO_2 single crystals were synthesized using a flux method, and x-ray diffraction determined that the orientation of the largest-area facet is (110). Mechanical polishing of the (110) surface resulted in a surface roughness of less than 0.1 nm. Using molecular beam epitaxy, single-crystalline rutile TiO_2 thin films were epitaxially grown on a (110) r-GeO_2 single-crystal substrate. Reflection high-energy electron diffraction (RHEED) determined that a 2D growth mode is maintained throughout the growth and the full width at half-maximum (FWHM) of the x-ray rocking curve of the TiO_2 thin films is 1.637°. Our results demonstrate the feasibility of our r-GeO_2 single-crystal substrates for epitaxial growth of rutile-type films.

II. EXPERIMENT

A. Flux synthesis of r-GeO_2 crystals

Quartz-phase GeO_2 [Puratronic®, 99.999% (metals basis), CAS 1310-53-8], MoO_3 [Alfa Aesar 99.95% (metals basis), CAS 1313-27-5], and Li_2CO_3 (ProChem Inc. ACS grade purity, CAS 554-13-2) were weighed in an approximate 1:16:10.5 molar ratio, with no drying or treatment of materials prior to reaction. Materials were loaded into a 30 ml Pt crucible (XRF Scientific, GC530). The crucible was loosely covered with a Pt lid and heated to 980 °C at a rate of 100 °C/h, where the temperature was held for 1 h and then cooled to 600 °C at rates of either 3, 1, or 0.5 °C/h, upon which the system was rapidly cooled to room temperature.

Crystals were extracted from the crucible by sonicating the flux in de-ionized water. The largest crystals were grown using the 0.5 °C/h cooling rate along with crystals from prior growths to serve as seeds.

B. Mechanical polishing

To planarize the surface with subnanometer roughness, the crystal surface was polished by mechanical polishing and abrasives. The crystal was first mounted on a polisher using a thinning fixture and mounting wax. The crystal surface was then ground using 6 μm, followed by 3 μm, and lastly 1 μm of diamond lapping films at the rotation speed of 30 rpm. After polishing with diamond lapping films, atomic force microscopy (AFM) measurement revealed that the pits on the crystal surfaces were removed but oriented scratches of up to 10 nm depth were left on the surfaces. Subsequently, to remove the finest scratches, the surface was ground again by using 0.05 μm aluminum oxide abrasive film disks, followed by Final Green™ films for the final step, at the rotation speed of 10 rpm for 1 h at each step.

C. Thin film deposition

To deposit TiO_2 thin film on r-GeO_2 crystals, an ozone source, which consists of ~15% O_3 and 85% O_2, is used as the oxidant and elemental titanium as a source material. Titanium was sublimed from a Ti-Ball at the flux of 1.2×10^{13} atoms/cm^2 s calibrated using a quartz crystal microbalance. The deposition temperature and the background pressure of the oxidant during the growth were kept at 450 °C and 1×10^{-6} Torr, respectively. The TiO_2 thin film was deposited for 12 h and monitored by RHEED. The estimated thickness of the TiO_2 thin film after 12 h of deposition is 72 nm.

III. RESULTS AND DISCUSSION

In most bulk crystal growth techniques, crystals are grown from a molten phase with a seed crystal as the starting material. The phase diagram of GeO_2, however, indicates that the quartz phase exists below the liquidus temperature, which precludes direct crystallization of the rutile phase.[26] With the flux method, we utilize a Li_2O–MoO_3 eutectic (derived from Li_2CO_3 and MoO_3 precursors)

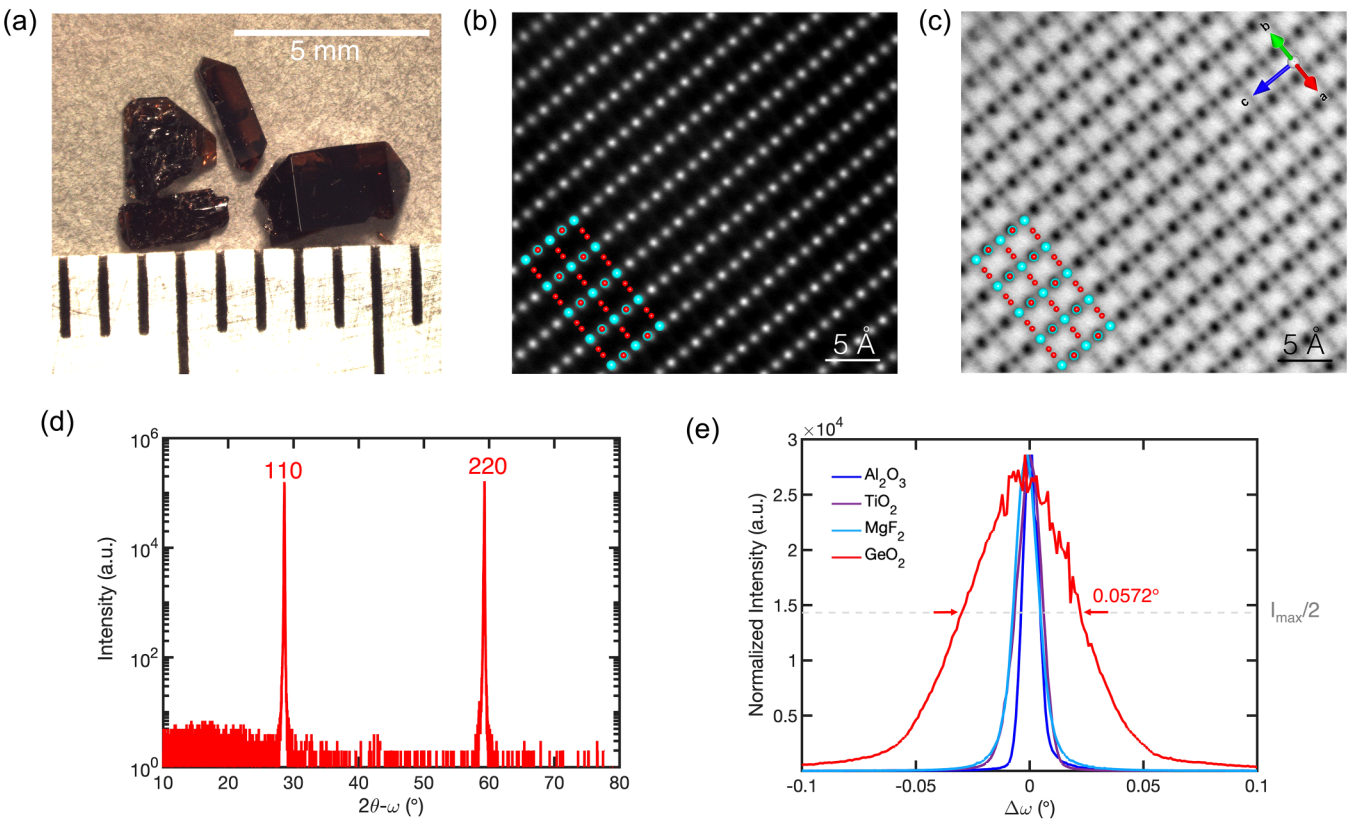

FIG. 2. Bulk crystallinity of rutile GeO_2 crystals. (a) Optical image of r-GeO_2 single crystals synthesized by the flux method. Crystal sizes reach up to 4 mm. (b) High-angle annular dark field and (c) annular bright field scanning transmission electron microscopy images of r-GeO_2 single crystals taken on the [110] zone axis. The overlay represents the rutile structure with blue and red dots representing Ge and O atoms, respectively, and corroborates the rutile structure. The *a* and *c* lattice parameters are 4.40 and 2.86 Å, respectively. (d) X-ray diffraction of r-GeO_2 single crystals with the largest-area facet oriented out-of-plane. (e) X-ray rocking curve of the GeO_2 110 diffraction peak compared with Al_2O_3 ($1\bar{1}02$), TiO_2 (110), and MgF_2 (001) single-crystal substrates purchased at MTI corporation.

which melts at conveniently low temperatures (~524 °C)[27] and dissolves GeO_2 as a solution at a temperature below the rutile-to-quartz transition temperature (~1050 °C) where the rutile is stable.[25] Upon slow cooling, the crystallization of the rutile phase occurs as the solution becomes critically supersaturated.[28] After crystal growth, the flux can be easily removed by dissolving in water leaving the resulting crystals (see Sec. II A for details).

Figure 2(a) shows the r-GeO_2 single crystals obtained by flux synthesis. The crystals have a plate-shape geometry consistent with the Wulff construction for rutile crystals and sizes ranging from 1 to 4 mm.[29] The scanning transmission electron microscopy images of an r-GeO_2 crystal in Figs. 2(b) and 2(c) show that all atomic columns including O are clearly visible in the high-angle annular dark field and annular bright field (ABF) images. The planar spacings of $(\bar{1}10)$ and (001) are measured to be 3.17 and 2.86 Å, respectively, which agree with the reported bulk lattice parameters of r-GeO_2.[30] Figure 2(d) plots x-ray diffraction measured for an r-GeO_2 crystal with the largest-area facet oriented parallel to the scattering vector. The peaks are measured at $2\theta = 28.61°$ and 59.31° which corresponds to the (110) family of planes of r-GeO_2. The miscut angle is less than 0.1°. In rutile the structure, the (110) plane has the lowest surface energy which explains the larger surface area. No other diffraction peaks are detected indicating that our r-GeO_2 crystals are single crystals without a noticeable impurity phase. To determine the crystalline quality of our crystals, the x-ray rocking curve of the 110 reflections of an r-GeO_2 crystal was measured and compared to sapphire, TiO_2, and MgF_2 substrates purchased from MTI corporation [Fig. 2(e)]. The FWHM of the x-ray rocking curve of the (110)-oriented r-GeO_2 single crystal was measured to be 0.0572° which is ~6.7 times wider than the $(1\bar{1}02)$ sapphire substrate (FWHM = 0.0085°) and ~4.4 times wider than the (110) TiO_2 and (001) MgF_2 substrates (FWHM = 0.013°). Though the FWHM of the x-ray rocking curve is wider than commercial substrates (probably due to the existence of impurities incorporated from solvent materials), the high degree of crystallinity motivates the preparation of the surface to the template epitaxial thin film growth.

The surface roughness of an as-grown r-GeO_2 crystal was measured by AFM in Fig. 3(a). The surface has a nanometer-range roughness with pits of ~300 nm width and ~4 nm depth along with small (12 nm diameter) particles. Figure 3(b) is the AFM image of an r-GeO_2 crystal after mechanical polishing. Mechanical polishing reduces the surface roughness from $R_q = 1.775$ nm to $R_q = 0.097$ nm, showing that an atomically smooth surface is achieved. The crystals were then annealed in a tube furnace to relieve any mechanical stress and repair surface crystallinity disrupted by the polishing step. The annealing condition was 700 °C for 3 h with 50 SCCM O_2 gas flowing at the atmospheric pressure. In Figs. 3(c) and 3(d), RHEED patterns are observed for the polished surface of an r-GeO_2 crystal at two different azimuths of [001] and $[\bar{1}10]$. The RHEED patterns show a streaky diffraction pattern and clear anisotropy consistent with the (110) rutile surface structure. Therefore, a single-crystalline surface is realized after mechanical polishing and postannealing, indicating a suitable substrate for epitaxial thin film growth.

To demonstrate the feasibility of epitaxial film growth on the prepared r-GeO_2 crystal, rutile TiO_2 thin films were grown on an r-GeO_2 substrate using molecular beam epitaxy. Figure 4(a) shows the x-ray diffraction $2\theta - \omega$ scan of a TiO_2 thin film on a (110)

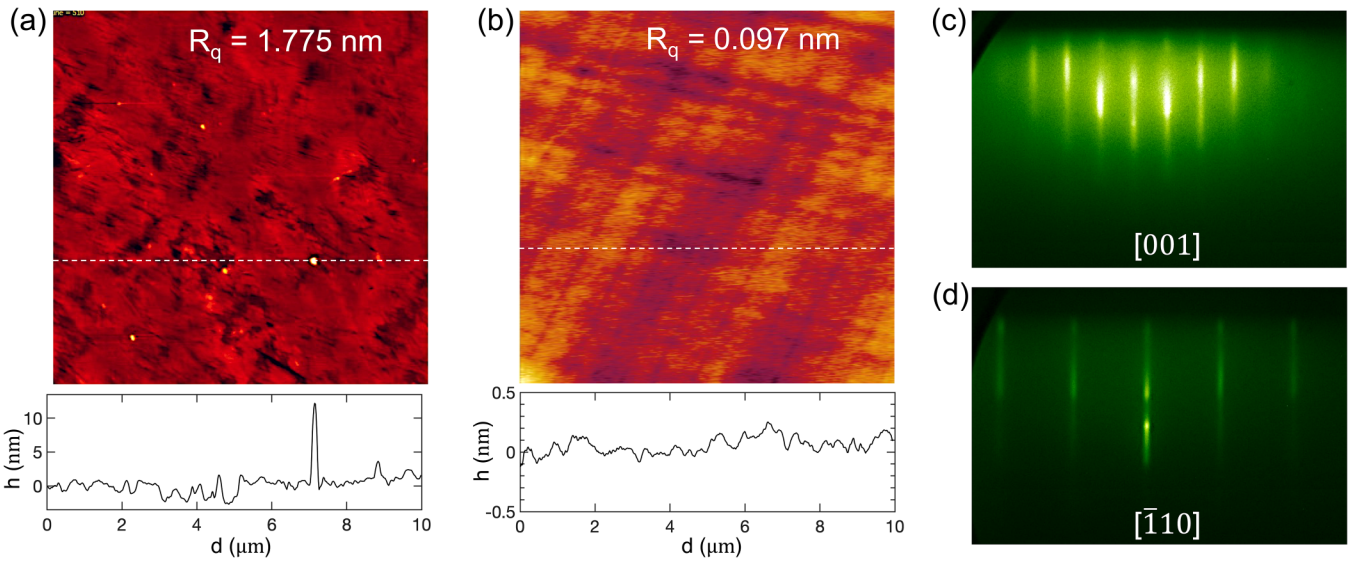

FIG. 3. Surface preparation of rutile GeO_2 single crystals. (a) and (b) Atomic force microscopy images of (a) as-grown r-GeO_2 single crystals and (b) r-GeO_2 single-crystal substrates after surface planarization by mechanical polishing and annealing. (c) and (d) Reflection high-energy electron diffraction patterns observed for the polished, post-annealed surface of an r-GeO_2 single-crystal substrate reveal a highly crystalline surface after preparation. The surface orientation is (110) and the azimuth is [001] for (c) and $[\bar{1}10]$ for (d).

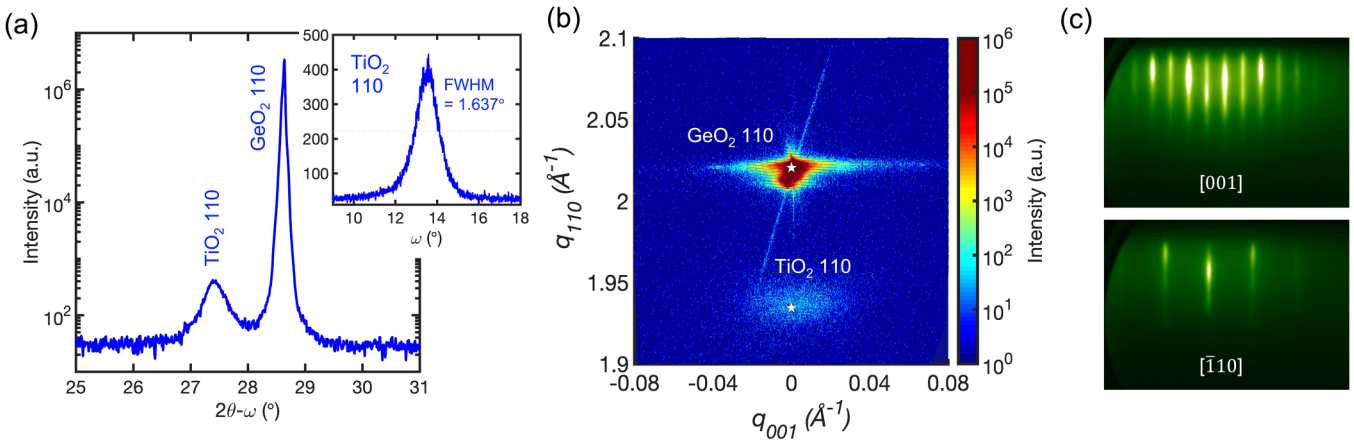

FIG. 4. TiO_2 film growth on a rutile GeO_2 substrate. (a) X-ray diffraction of an epitaxial TiO_2 thin film grown on a (110)-oriented r-GeO_2 substrate. The inset shows the rocking curve of the indicated TiO_2 film peak. (b) A symmetric reciprocal space map around the 110 reflections of the TiO_2 thin film on the r-GeO_2 substrate. (c) Reflection high-energy electron diffraction patterns observed for TiO_2 thin films grown on a (110) r-GeO_2 substrate recorded at the [001] and [$\bar{1}$10] azimuths.

r-GeO_2 substrate with the x-ray rocking curve of the TiO_2 thin film as an inset. In Fig. 4(a), a strong diffraction peak was observed for the TiO_2 thin film which corresponds to the (110) orientation of rutile TiO_2 and demonstrates the epitaxial growth of a TiO_2 thin film on an r-GeO_2 substrate. The FWHM of the rocking curve of the TiO_2 thin film was measured to be 1.637°. We attribute the relatively wide rocking curve of our film to low deposition temperature compared to other reports[31–33] where highly crystalline films are obtained. Another potential source of degraded crystallinity may be from Mo impurities from the r-GeO_2 substrate. The symmetric reciprocal map in Fig. 4(b) shows that the out-of-plane lattice spacing of an r-TiO_2 thin film on an r-GeO_2 substrate is close to the bulk lattice spacing as indicated with the star marker on the plot, which indicates strain relaxation of the TiO_2 thin film.

Figure 4(c) shows RHEED images of an r-TiO_2 thin film on the r-GeO_2 substrate after 12 h of deposition. Throughout the deposition of TiO_2 on an r-GeO_2 substrate, streaky-spotty diffraction is observed, and the spots appeared even sharper compared to the bare substrate surface before deposition. Our result demonstrates the templating effect of the r-GeO_2 substrate, which can potentially be applied for the epitaxial stabilization of rutile thin films that are challenging to stabilize on known substrates.

IV. SUMMARY AND CONCLUSIONS

In conclusion, (110)-oriented r-GeO_2 single-crystal substrates were fabricated by flux synthesis and mechanical polishing. The new substrates provide access to a previously inaccessible region of lattice parameter and strain space for rutile thin films. The size of the largest r-GeO_2 substrate is around 10 mm^2 and exhibits excellent crystallinity. The FWHM of the rocking curve of a substrate is 0.057°. Following a mechanical polishing and anneal process, a crystalline (110) surface of the r-GeO_2 substrate exhibits a roughness of $R_q < 0.1$ nm. To demonstrate possibilities for thin film epitaxy, epitaxial r-TiO_2 thin films were grown on these newly developed (110)-oriented r-GeO_2 substrates using reactive molecular beam epitaxy. We observed sharp, streaky diffraction of the RHEED throughout the deposition of r-TiO_2 thin films, showing that our r-GeO_2 substrates support epitaxial growth of r-TiO_2 thin films with excellent crystallinity. While the synthesis times and small crystal sizes make it unlikely that this process will directly lead to larger and commercialize substrates, we posit that they can serve as seeds for scaled-up (cm-scale) crystal synthesis techniques, such as top seeded solution growth, that are more amenable for commercialization.

ACKNOWLEDGMENTS

This work was supported by the National Science Foundation [Platform for the Accelerated Realization, Analysis, and Discovery of Interface Materials (PARADIM)] under Cooperative Agreement No. DMR-2039380. S.C. acknowledges support from Rackham Predoctoral Fellowship. This work made use of the Cornell Center for Materials Research (CCMR) Shared Facilities, which are supported through the NSF MRSEC Program (No. DMR-1719875). The Thermo Fisher Helios G4 UX FIB was acquired with support by NSF No. DMR-1539918. The Thermo Fisher Spectra 300 X-CFEG was acquired with support from PARADIM and Cornell University.

AUTHOR DECLARATIONS

Conflict of Interest

The authors have no conflicts to disclose.

Author Contributions

Sieun Chae: Conceptualization (equal); Data curation (equal); Formal analysis (equal); Investigation (equal); Writing – original draft (equal). **Lucas A. Pressley:** Formal analysis (equal); Investigation (equal); Methodology (equal); Resources (equal).

Hanjong Paik: Conceptualization (equal); Investigation (equal); Project administration (equal); Resources (equal). **Jiseok Gim:** Formal analysis (equal); Investigation (equal); Methodology (equal); Resources (equal). **Don Werder:** Formal analysis (equal); Investigation (equal); Methodology (equal); Resources (equal). **Berit H. Goodge:** Formal analysis (equal); Investigation (equal); Methodology (equal); Resources (equal). **Lena F. Kourkoutis:** Funding acquisition (equal); Project administration (equal); Resources (equal); Supervision (equal). **Robert Hovden:** Investigation (equal); Methodology (equal); Resources (equal). **Tyrel M. McQueen:** Funding acquisition (equal); Investigation (equal); Methodology (equal); Project administration (equal); Resources (equal); Supervision (equal). **Emmanouil Kioupakis:** Conceptualization (equal); Investigation (equal); Project administration (equal); Resources (equal); Supervision (equal). **John T. Heron:** Conceptualization (equal); Investigation (equal); Project administration (equal); Resources (equal); Supervision (equal); Writing – review & editing (equal).

DATA AVAILABILITY

The data that support the findings of this study are available from the corresponding author upon reasonable request. Raw data from the facility related to these syntheses are generated at PARADIM large scale facility and are available after publication at https://data.paradim.org/.

REFERENCES

[1]Z. Hiroi, Prog. Solid State Chem. **43**, 47 (2015).
[2]N. Shukla, A. V. Thathachary, A. Agrawal, H. Paik, A. Aziz, D. G. Schlom, S. K. Gupta, R. Engel-Herbert, and S. Datta, Nat. Commun. **6**, 7812 (2015).
[3]M. Grätzel, Nature **414**, 338 (2001).
[4]M. Planells, L. Pellejá, J. N. Clifford, M. Pastore, F. De Angelis, N. López, S. R. Marder, and E. Palomares, Energy Environ. Sci. **4**, 1820 (2011).
[5]N. López, J. D. Prades, F. Hernández-Ramírez, J. R. Morante, J. Pan, and S. Mathur, Phys. Chem. Chem. Phys. **12**, 2401 (2010).
[6]Y. Lee, J. Suntivich, K. J. May, E. E. Perry, and Y. Shao-Horn, J. Phys. Chem. Lett. **3**, 399 (2012).
[7]S. Cherevko *et al.*, Catal. Today **262**, 170 (2016).
[8]S. A. Howard, E. Evlyukhin, G. Páez Fajardo, H. Paik, D. G. Schlom, and L. F. J. Piper, Adv. Mater. Interfaces **8**, 2001790 (2021).
[9]E. E. Benson, E. M. Miller, S. U. Nanayakkara, D. Svedruzic, S. Ferrere, N. R. Neale, J. Van de Lagemaat, and B. A. Gregg, Chem. Mater. **29**, 2173 (2017).
[10]J. P. Ruf *et al.*, Nat. Commun. **12**, 1 (2021).
[11]W. Zhou, Y. Liu, Y. Yang, and P. Wu, J. Phys. Chem. C **118**, 6448 (2014).
[12]E. E. Benson, M. A. Ha, B. A. Gregg, J. van de Lagemaat, N. R. Neale, and D. Svedruzic, Sci. Rep. **9**, 15906 (2019).
[13]W. Liu *et al.*, ACS Appl. Mater. Interfaces **12**, 47010 (2020).
[14]S. A. Chambers and Y. Liang, Surf. Sci. **420**, 123 (1999).
[15]S. Dwivedi and S. Biswas, Thin Solid Films **655**, 13 (2018).
[16]J. H. Kwon, Y. H. Choi, D. H. Kim, M. Yang, J. Jang, T. W. Kim, S. H. Hong, and M. Kim, Thin Solid Films **517**, 550 (2008).
[17]K. Fukushima, G. H. Takaoka, and I. Yamada, Jpn. J. Appl. Phys. **32**, 3561 (1993).
[18]S. Chae, H. Paik, N. M. Vu, E. Kioupakis, and J. T. Heron, Appl. Phys. Lett. **117**, 072105 (2020).
[19]S. Chae *et al.*, Appl. Phys. Lett. **118**, 260501 (2021).
[20]S. Chae, J. Lee, K. A. Mengle, J. T. Heron, and E. Kioupakis, Appl. Phys. Lett. **114**, 102104 (2019).
[21]H. Okamoto, J. Phase Equilib. Diffus. **32**, 473 (2011).
[22]U. Balachandran and N. G. Eror, J. Mater. Sci. **23**, 2676 (1988).
[23]A. T. Dinsdale, A. Akhmetova, A. V. Khvan, and N. Aristova, J. Phase Equilib. Diffus. **36**, 254 (2015).
[24]V. Agafonov, M. Michel, A. Kahn, M. Perez, and Y. Jorba, J. Cryst. Growth **71**, 12 (1985).
[25]J. W. Goodrum, J. Cryst. Growth **7**, 254 (1970).
[26]M. Micoulaut, L. Cormier, and G. S. Henderson, J. Phys.: Condens. Matter **18**, R753 (2006).
[27]M. Moser, D. Klimm, S. Ganschow, A. Kwasniewski, and K. Jacobs, Cryst. Res. Technol. **43**, 350 (2008).
[28]D. E. Bugaris and H. C. Zur Loye, Angew. Chem. Int. Ed. **51**, 3780 (2012).
[29]F. Jiang, L. Yang, D. Zhou, G. He, J. Zhou, F. Wang, and Z. G. Chen, Appl. Surf. Sci. **436**, 989 (2018).
[30]W. H. Baur and A. A. Khan, Acta Crystallogr. Sect. A Struct. Crystallogr. Crystal Chem. **27**, 2133 (1971).
[31]H. Lin, A. K. Rumaiz, M. Schulz, D. Wang, R. Rock, C. P. Huang, and S. I. Shah, Mater. Sci. Eng. B **151**, 133 (2008).
[32]E. Kumi-Barimah, R. Penhale-Jones, A. Salimian, H. Upadhyaya, A. Hasnath, and G. Jose, Sci. Rep. **10**, 10144 (2020).
[33]P. J. Hansen, V. Vaithyanathan, Y. Wu, T. Mates, S. Heikman, U. K. Mishra, R. A. York, D. G. Schlom, and J. S. Speck, J. Vac. Sci. Technol. B**23**, 499 (2005).